Hauschildt, K.; Stark, A.; Schell, N.; Mueller, M.; Pyczak, F.:
The transient liquid phase bonding process of a Gamma-TiAl alloy with brazing solders containing Fe or Ni.
In: Intermetallics. Vol. 106 (2019) 48 - 58.
(DOI: /10.1016/j.intermet.2018.12.004)
First published online by Elsevier: 18.12.2018

https://dx.doi.org/10.1016/j.intermet.2018.12.004

The transient liquid phase bonding process of a γ-TiAl alloy with brazing solders containing Fe or Ni

Katja Hauschildt, Andreas Stark, Norbert Schell, Martin Müller, Florian Pyczak

All: Helmholtz-Zentrum Geesthacht, Max-Planck-Strasse 1, 21502 Geesthacht

Abstract

The high Nb-containing γ-TiAl alloy Ti-45Al-5Nb-0.2B-0.2C (in at. %) was successfully brazed by transient liquid phase (TLP) bonding using two brazing solders with different melting point depressing elements (MPD): Ti-24Ni and Ti-29Fe (in at. %). The brazing process was executed for 24 h at 1110 °C. An additional annealing was performed for 168 h at 1000 °C for a better homogenization. The joints were characterized with high-energy X-ray diffraction (HEXRD) and scanning electron microscopy (SEM) using energy dispersive X-ray spectroscopy (EDX). Depending on the MPD and if the specimens were annealed two to three symmetrically arranged transition zones developed between the substrate and the middle of the joint with different microstructures, phase compositions, and chemical compositions. Beside α_2 and γ which have been present in the substrate additional phases as β, β_o, ω_o, τ_3, and τ_2 were identified in the joints. We discuss the different solidification paths and the following solid-state transformations. The Fe-containing joint solidified via a single β_o phase field leading to large β_o grains. In contrast, the Ni-containing joint solidified via a two-phase field resulting in a finer grained microstructure.

Keywords

A. intermetallics; B. diffusion, phase transformation; C. joining; D. microstructure; F. X-ray diffraction

1. Introduction

TiAl alloys were recently introduced as an alternative to Ni-base superalloys for low-pressure turbine blades in aero engines [1-3]. The benefits are twofold. Due to their higher specific strength compared to Ni-base superalloys engine efficiency is increased and due to their lower density the overall weight is reduced. Still some major improvements are desirable for a broader application of TiAl alloys. An example is the improvement of ductility and damage tolerance of parts made of TiAl, which are extremely sensitive to the microstructure [1, 2]. TiAl alloys are composed of ordered intermetallic phases: γ-TiAl, α_2-Ti_3Al and sometimes β_o-TiAl [1, 2]. To improve the strength and creep resistance of TiAl alloys the amount of niobium is increased to levels between 5 and 8 at. % while in parallel the aluminum content is decreased to 45 at. % or below and precipitation hardeners such as boron and carbon are added [1]. The addition of boron as well as Nb also improves the processability of the alloy [1, 2]. These so called third generation alloys exhibit a good combination of high strength and ductility. However, their ductility and damage tolerance suffer even more from coarse or inhomogeneous microstructures than second generation TiAl alloys with lower strength as for example Ti-48Al-2Cr-2Nb [1, 2]. Usually, only hot working processes like hot extrusion or forging provide a sufficient microstructure homogeneity to result in a good combination of strength and ductility for the third generation TiAl alloys.

Today turbine blades made from Ni-base alloys usually undergo a number of refurbishment cycles before they are fully replaced [3]. Transient liquid phase (TLP) bonding is a well-established repair

method for the crack closure of Ni-base superalloys [3-6]. The fact that cracks in single crystal superalloys are closed by a single crystalline braze zone using TLP bonding illustrates the high microstructural homogeneity between substrate and braze zone achievable by this process [3, 6-8]. To save cost and resources similar repair procedures should also be established for parts made of TiAl alloys [9]. Due to the high sensitivity of the mechanical properties of TiAl parts to the microstructure already mentioned earlier it is clear that any repair process for TiAl parts should produce a fine homogeneous microstructure in the repaired zone and retain the microstructure of the surrounding material. This makes TLP bonding attractive as in principle it should be possible to fully homogenize the chemical composition between the braze zone and the substrate material. There are several publications on this topic for γ-TiAl alloys [10-13], but usually the brazing time is in the range of less than one hour, which most probably is too short for chemical and microstructural homogenization by diffusion processes [10, 13]. Additionally, pressure was applied on the specimens in some experiments [10], which would be not applicable i.e. for a repair process of cracks in machined parts.

The idea of TLP bonding, also known as diffusion brazing [14], is to use a braze alloy composed of elements present in the substrate and an additional alloying element, which reduces the melting point of the braze alloy, called melting point depressing element (MPD). The combination of substrate and braze alloy is heated to a temperature above the melting point of the braze alloy but below the melting point of the substrate material. During holding at that temperature, the MPD diffuses into the substrate material. As a consequence, the content of MPD decreases and thus the melting point of the material increases continuously in the braze zone. After a sufficient holding time the material in the braze zone solidifies because its melting point has risen above the brazing temperature. In contrast to conventional brazing processes the chemical composition between braze zone and substrate material is homogenized during TLP bonding, resulting in a more homogenous microstructure. However, chemical homogenization to the point when the joint region solidifies is not necessarily sufficient to ensure that the microstructure of the braze joint and substrate material do not differ anymore.

In the present paper a TLP bonding process for a third generation TiAl alloy is reported using either Fe or Ni as MPD. We use binary eutectic compositions with Ti for the brazing solders due to their low melting points. Thus, the brazing temperature can be chosen relatively low in comparison to the melting points of the substrate which should restrict grain coarsening. To our knowledge, such a long brazing time (24 h), and thus time for homogenization, has been investigated for the first time for TiAl alloys. Also the effects of an additional annealing treatment were investigated. The microstructures of the joints were investigated with scanning electron microscopy (SEM) using energy dispersive X-ray spectroscopy (EDX). Furthermore, they were scanned stepwise with a fine high-energy X-ray beam. Subsequently, the high-energy X-ray diffraction (HEXRD) data were characterized by a Rietveld refinement to determine the phase composition space-resolved. Additionally, we discuss the microstructural development of the two different systems and compare them.

2. Experimental

As a substrate material for the brazing tests the TiAl alloy TNB-V5 (Ti-45Al-5Nb-0.2B-0.2C in at. %) was used in hot extruded condition processed by the company Special Metals Wiggin Ltd, Hereford,

United Kingdom. The Ti-rich eutectic compositions Ti-24Ni and Ti-29Fe (in at. %) were chosen as braze alloys with the melting points of 942 °C and 1078 °C, respectively [15, 16]. They were produced in-house in an arc melting furnace and were remelted several times to ensure homogeneity.

For brazing experiments the TiAl substrate was cut in blocks of approximately (10x10x5) mm^3. From the braze alloys thin foils with a thickness of about 300 µm and the same base area as the substrate material were prepared by cutting and grinding. Prior to brazing the surfaces of the braze foil as well as the substrate material were ground using 320 grit SiC-paper. Subsequently, the specimens were cleaned ultrasonically. For the brazing process two TNB-V5 blocks were stacked with a foil of the brazing solder in between. The specimens were brazed in a vacuum furnace for 24 h at 1110 °C under a pressure of 10^{-5} mbar. They were heated up to the brazing temperature in 1 h and furnace cooled after the brazing process. Subsequently to the 24 h brazing process a set of specimens was annealed for 168 h at 1000 °C in air and furnace cooled in order to investigate the effects of an additional annealing.

For microstructure characterization specimens were cut perpendicular to the brazing joint and ground with SiC-paper up to 2500 grit. Afterwards, the specimens were vibration or electrolytically polished. The vibration polishing was executed for about 24 h and the electrolytic polishing was performed with a voltage of 37.5 V at -47 °C with an agent of 600 ml methanol, 300 ml butanol, and 60 ml perchloric acid. All micrographs were recorded by a Leo Gemini SEM equipped with a field emission gun using back scattered electrons (BSE). To determine the chemical composition of the braze zones an EDAX EDX system was used with an acceleration voltage of 20 kV. An EDX area mapping of the whole joint with adjacent substrate was executed. Therein, regions of interest were chosen fitting with the different zones of the microstructure and with a length of 500 µm or 750 µm parallel to the joint for the as-brazed and the annealed specimens respectively. The summed EDX profiles in each region were evaluated with the proprietary software suite of the system EDAX Genesis. The TiAl substrate far away from the joint and thus without any influence of the MPD was used as a standard for the EDX measurements. Mean errors for the single elements were determined for Ti to be 0.9 at. %, for Al to be 2.2 at. %, for Nb to be 0.1 at. %, and for Ni to be 0.1 at. %.

For HEXRD measurements, a slice of about 1 mm thickness was cut of the brazed specimens perpendicular to the brazing joint. The HEXRD measurements were performed at the High-Energy Materials Science Beamline (HEMS/P07) of Helmholtz-Zentrum Geesthacht at the PETRA III synchrotron radiation facility at DESY (Deutsches Elektronen-Synchrotron), Hamburg, Germany [17]. The specimens were measured in transmission with an energy of 87.1 keV, corresponding to a wavelength of 0.014235 nm. A higher harmonic wavelength due to the experimental setup led to some known additional Bragg reflections. A mar345 image plate detector or a PerkinElmer XRD1621 flat panel detector were used to record the diffraction patterns of the as-brazed and the annealed specimens, respectively. Fig. 1 shows quarters of the Debye-Scherrer diffraction patterns of measurements out of the middle of the as-brazed Fe-containing (1a) and the as-brazed Ni-containing (1b) joint. The specimens were scanned over the horizontally aligned brazing joint using a beam that was 100 µm in width and 50 µm in height with a step width of 25 µm. Each area was exposed for 40 seconds, in total 21 vertically aligned neighbouring (overlapping) regions were scanned. During the scanning process the specimens were rotated 60° around the vertical axis. This resulted in diffraction information from a higher number of grains which were tilted into diffraction condition. The recorded Debye-Scherrer rings were integrated over 360° azimuthal angle and displayed as a function of the 2Θ angle or the scattering vector q with the program Fit2d [18]. Two integrated

diffractograms out of the middle of the joint are shown in fig. 1c and d below the respective Debye-Scherrer diffraction patterns. Afterwards, a Rietveld refinement was executed with the ideal stoichiometric structures of the phases (see the appendix) using the software MAUD (Materials Analysis Using Diffraction) [19].

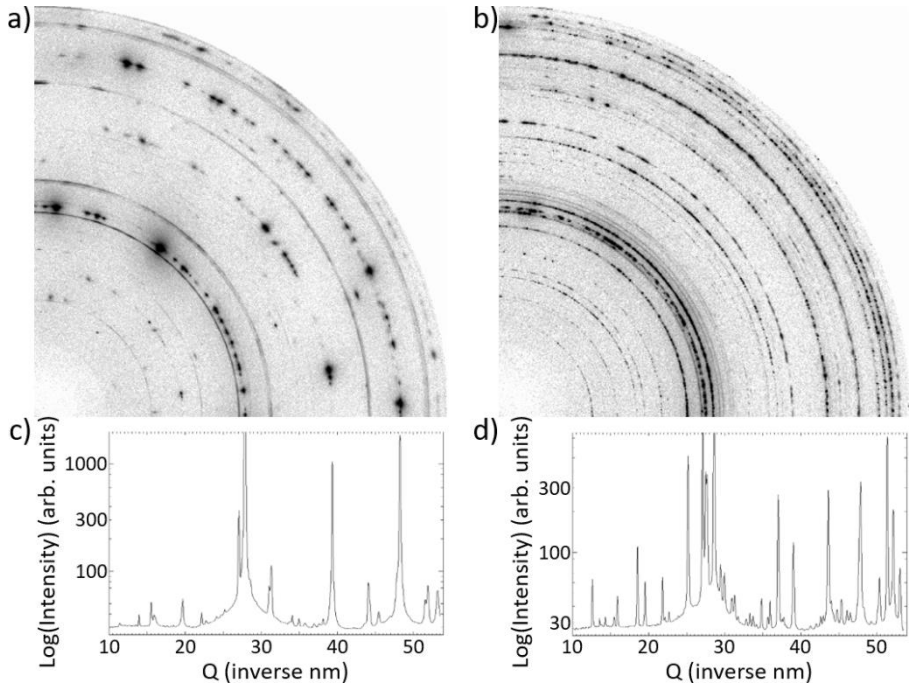

Fig. 1: Quarters of the Debye-Scherrer diffraction patterns from measurements out of the middle of the as-brazed Fe-containing (a) and the as-brazed Ni-containing (b) joint. The respective integrated diffractograms are shown below (c and d).

3. Results and Discussion

3.1 Initial materials

For the brazing process, a brazing temperature has to be chosen, at which no significant changes in the microstructure of the substrate take place while still being as high as possible to allow fast chemical homogenization by diffusion. Therefore, we selected 1110 °C as brazing temperature. The microstructure of the initial substrate, the hot extruded material, is shown in fig. 2a. It consists mainly of fine dynamically recrystallized γ and α_2 grains and a few coarse lamellar (α_2+γ) colonies. As shown in fig. 2b, the microstructure coarsened slightly after an annealing for 24 h at 1110 °C but the γ and α_2 grain size still remained fine (< 10 µm). As determined by Rietveld refinement, the substrate material consists of about 80 vol. % γ phase, 19 vol. % α_2 phase, and 1 vol. % TiB phase [1]. The eutectic brazing solders consist of about 57 vol. % β-Ti and 43 vol. % FeTi phase for Ti-29Fe [16] and 69 vol. % Ti_2Ni and 31 vol. % α-Ti phase for Ti-24Ni [15]. An overview of the crystallographic data of these phases together with crystallographic data of all phases found in the joints are compiled in the appendix.

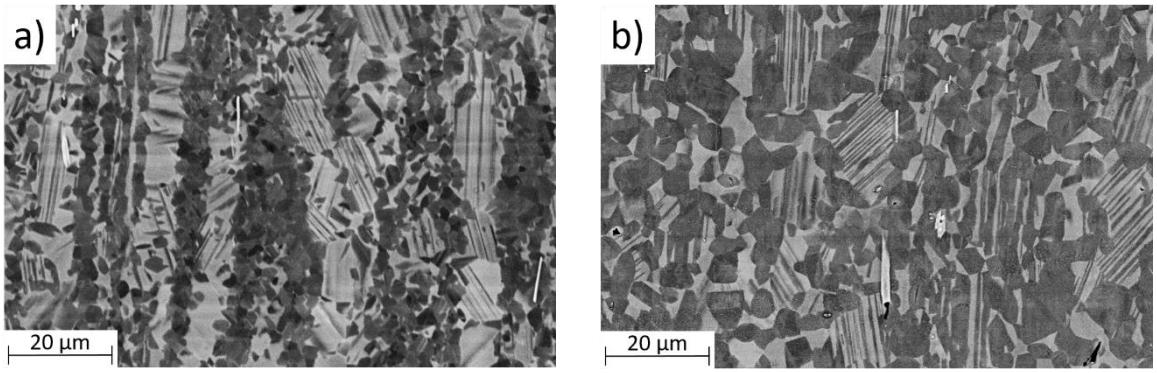

Fig. 2: Microstructure of the substrate material Ti-45Al-5Nb-0.2B-0.2C: a) as-extruded, b) after an annealing at 1110 °C.

3.2 Results Fe-based solder – as-brazed condition

3.2.1 Microstructure

The microstructure of the joint differs clearly from the substrate. The elements Ni and Fe which are enriched in the joint result in a brighter contrast of this region in the BSE SEM micrographs. Thus, in the following sections, this brighter region in the microstructure is identified with the joint consisting of two to three different zones. And the region which appears darker is named substrate usually with a diffusion affected zone next to the joint. As shown in fig. 3a the microstructure of the as-brazed specimen shows two zones in the joint (I: middle and II: transition zone) and a zone with diffusion affected substrate (zone III) next to the joint and the substrate (substr.). These transition zones are symmetric on both sides of the joint. The joint region possesses a width of about 275 µm and shows no pores or cracks. As already mentioned, the joint appears much brighter than the substrate in BSE mode due to the higher amount of the heavy elements Fe and Ti compared to the substrate. In detail, the middle of the joint shows two rows of large, blocky β_o grains each with a width of about 100 µm and a length of more than 100 µm. Additionally, dark needles or platelets of γ phase are embedded, and it seems that the β_o grains are surrounded by a γ seam. Thus, a dark seam is visible along the joint in the middle of the joint. In the transition zone additional light grey globular grains (α_2 phase) are visible. Next to the joint in zone III the grains of the diffusion affected substrate appear bigger than in the substrate further away from the joint.

3.2.2 Phase analysis with HEXRD

The amount of γ decreases continuously from the diffusion affected substrate to the middle of the joint from 80 to 11 vol. %, fig. 3b. Furthermore, the amount of α_2 phase also starts to decrease in the diffusion affected substrate, increases slightly in the transition zone and is almost absent (2 vol. %) in the middle of the joint. The amount of β_o+ω" increases significantly from 0 to 87 vol. % in the middle of the joint. A diffraction pattern recorded in the middle of the joint (fig. 4) shows superstructure reflections of β_o and ω" besides β main reflections [20]. However, the intensity of the β_o superstructure reflections is too weak to indicate an ideally ordered stoichiometric β_o-TiAl structure. All peaks of the ω" phase could be identified in the diffraction data, but no distinct splitting of the main peak (q=27.8 nm^{-1}) which is also associated with the presence of ω" phase is visible. Additionally, the ω" peaks are significantly broadened compared to the single peaks of the β_o and γ phase.

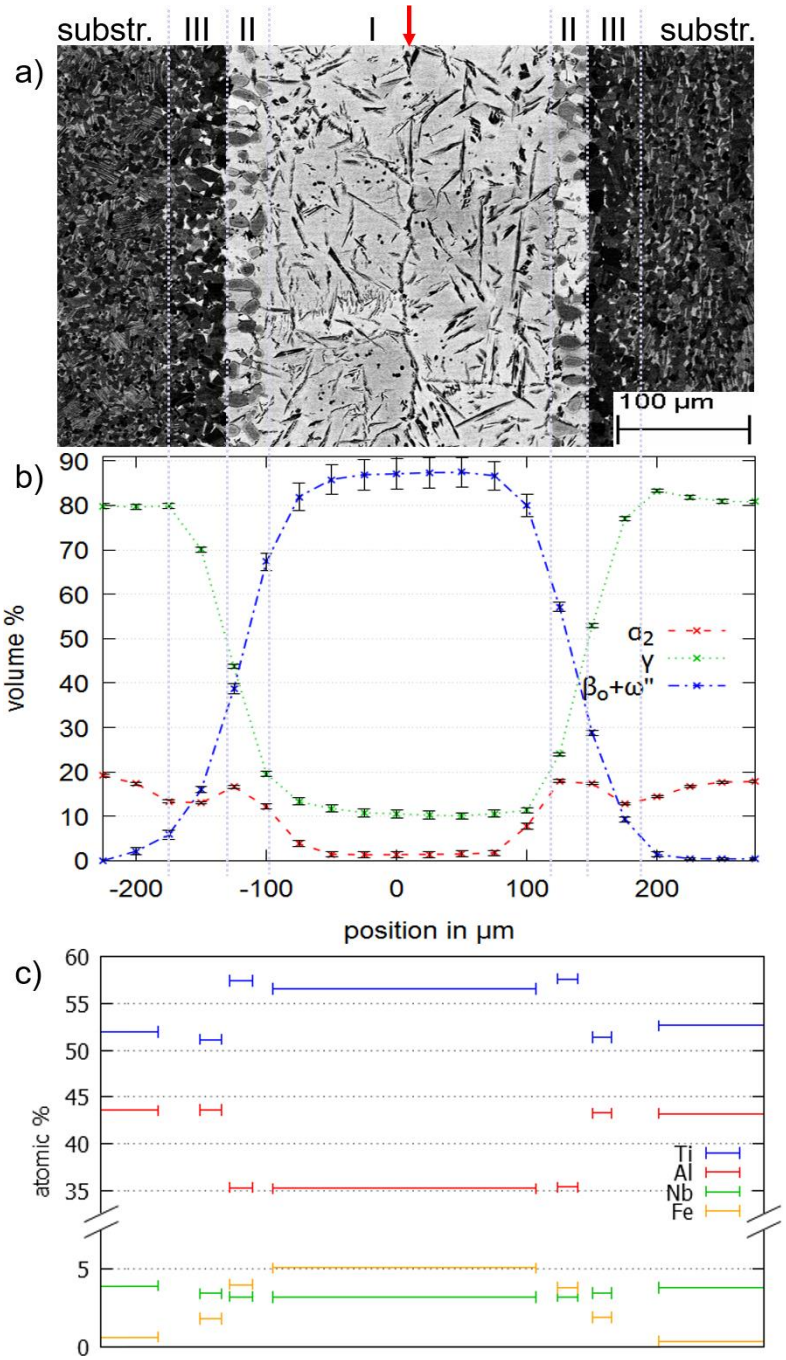

Fig. 3: The results of the Fe-containing as-brazed specimen arranged next to each other a) Microstructure, b) Volume fractions of phases determined by Rietveld analysis of HEXRD measurements, and c) Results of the EDX mappings. The different zones are marked: substr.: substrate, zone I: middle, zone II: transition zone, zone III: diffusion affected substrate. The red arrow marks the middle of the joint.

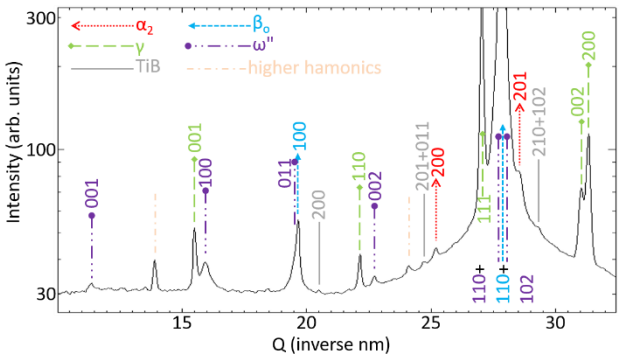

Fig. 4: Diffraction pattern from the middle of the Fe-containing as-brazed joint showing peaks of α_2, γ, TiB, β_o, and ω" phase and some weak peaks which can be attributed to the higher harmonic wave length at the beamline.

3.2.3 Chemical analysis (EDX)

In fig. 3c results of an EDX mapping over the joint of the as-brazed specimen are shown. The amounts of Al and Nb increase from the middle of the joint to the substrate. It is noteworthy that the content of Al is already at 35.2 at. % in the middle of the joint, while the brazing solder initially contained no Al. Also the content of Nb only slightly increases towards the substrate as 3.2 at. % was measured in the middle of the joint. The amount of Fe decreases from the middle of the joint to the substrate, due to the initial composition of the brazing solder being rich in this element. The local changes of the Ti concentration show a more discontinuous behaviour. Noticeably, the average amount of Ti increases from zone I (middle) to zone II and decreases clearly to zone III, but increases again slightly to the substrate. On the other hand, the amount of Fe continuously decreases from the middle of the joint to the substrate over the different zones. Remarkably, a high amount of Fe has already diffused into the substrate because only an average of 5.5 at. % Fe remains in the middle of the joint. The Fe is homogeneously distributed over the whole bright middle zone (i.e. the phase enclosing the dark needles). The composition of the diffusion affected substrate is almost the same as of the microstructurally unaffected substrate with the exception of the amount of Fe which has increased to 1.8 at. %. At least, the chemical composition of the microstructurally unaffected substrate compared to the initial composition (Ti-45Al-5Nb-0.2B-0.2C) shows a diffusion of Al and Nb into and of Fe and Ti out of the joint, but here the microstructure apparently did not change.

3.3 Results Fe-based solder - annealed condition

3.3.1 Microstructure

At the first glance the microstructure of the brazing joint with the Ti-29Fe brazing solder, fig. 5a, changes not significantly after the annealing in comparison to the as-brazed specimen, but the joint region widens from 275 µm to 400 µm. Especially, the transition zone II seems to become more than twice as wide during the annealing. The width of the diffusion affected substrate (zone III) decreases and is hardly distinguishable from the substrate. Still, there are no pores or cracks visible in the joint. The blocky β_o grains in zone I still appear with a width of about 100 µm. However, more dark γ grains are visible, which partly exhibit a more globular form. There is still no α_2 phase visible. In zone II the

microstructure exhibits globular grains in a similar size as before annealing. Additionally, more α_2 grains (light grey) are visible after the annealing in zone II.

3.3.2 Phase analysis with HEXRD

After annealing the detected phases are the same as in the as-brazed specimen, fig. 5b. Nevertheless, the phase composition adapts more to the substrate with decreasing β_o+ω" content and increasing γ and α_2 contents. In detail, the content of β_o+ω" decreases by almost 20 vol. % in the middle. As in the as-brazed specimen, peaks of ω" are visible besides β_o phase. It should be noted that the full-width-at-half-maximum (FWHM) of the superstructure peaks of ω" is almost reduced by half in comparison to the as-brazed specimen (not shown here). Additionally, in the middle the amounts of γ and α_2 phase have more than doubled after the annealing from 11 vol. % to 25 vol. % and from 2 vol. % to 5 vol. %, respectively. Furthermore, after annealing the amount of α_2 phase increases in the transition zone to 30 vol. % which is even above the level of the substrate. This correlates with the widening of the transition zone in the microstructure.

3.3.3 Chemical analysis (EDX)

After annealing, the chemistry between the joint and the substrate is better homogenized due to diffusion, fig. 5c. This means, in comparison to the as-brazed specimen, that the amounts of Al and Nb increase in the middle of the joint. Accordingly, the amount of Ti decreases. Remarkably, the amount of the MPD Fe is still nearly the same in the middle of the joint as prior to the annealing process. Furthermore, after annealing the microstructurally unaffected substrate shows nearly the same composition as the initial substrate in contrast to the as-brazed specimen where the influence of the diffusion into the substrate is noticeable.

3.4 Discussion Fe-based solder

The widening of the joint region after the annealing shows that diffusion is still significant during the annealing. After the annealing, the chemical composition is better homogenized but still differs clearly from the substrate. Thus, the diffusive homogenisation is not fully completed.

The phase compositions after brazing can be explained with the ternary phase diagrams of Al-Fe-Ti at 1000 °C and 1200 °C from [21]. The respective phase diagram at 1000 °C is shown in fig. 6. No liquid region is reported there, but it exists at the brazing temperature of 1110 °C in the region of the composition of the brazing solder. A flow chart of the transformation path of the whole joint is shown in fig. 7a. When reaching the melting point of the brazing solder the material liquefies and solves the adjacent substrate. While the temperature remains constant, the chemical composition changes continuously. Hence, the chemical composition in the middle of the joint (zone I) moves to the binary phase field L+β in the direction of increasing Al and decreasing Ti and Fe contents. Thus, β grains grow on both sides of the substrate. After comparison with the ternary phase diagram at 1200 °C from Palm et al. [21] we assume that the β phase is initially disordered at the brazing temperature of 1110 °C. Subsequently, further changes in the chemical composition due to diffusion do not influence the phase composition much, as the β phase field appears rather big in the ternary phase diagram. Thus, after the joint fully solidifies, the composition is placed within the single β phase field.

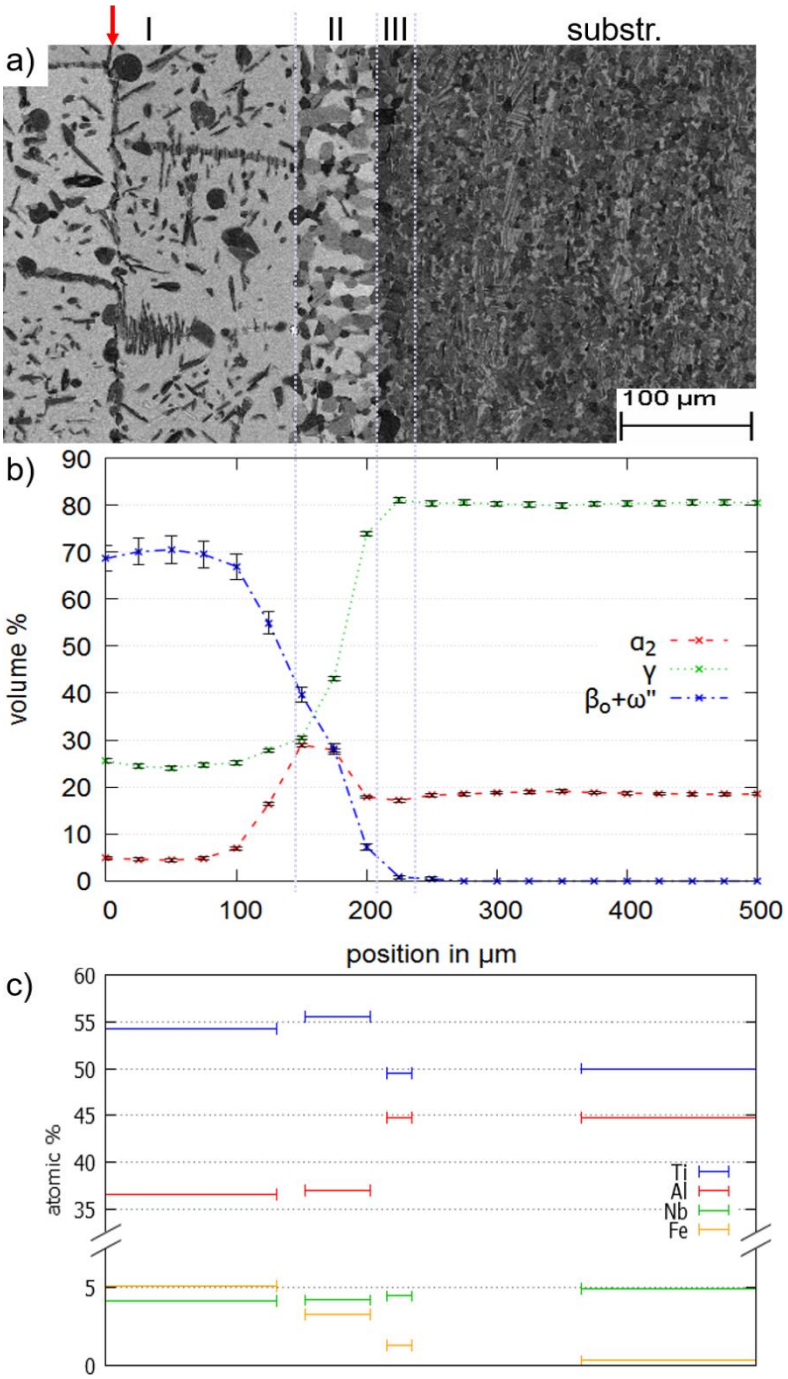

Fig. 5: The results of the Fe-containing annealed specimen arranged next to each other a) Microstructure, b) Volume fractions of phases determined by Rietveld analysis of HEXRD measurements, and c) Results of the EDX mappings. The different zones are marked: substr.: substrate, zone I: middle, zone II: transition zone, zone III: diffusion affected substrate. Only half of the joint was analysed and is shown here, the red arrow marks the middle of the joint.

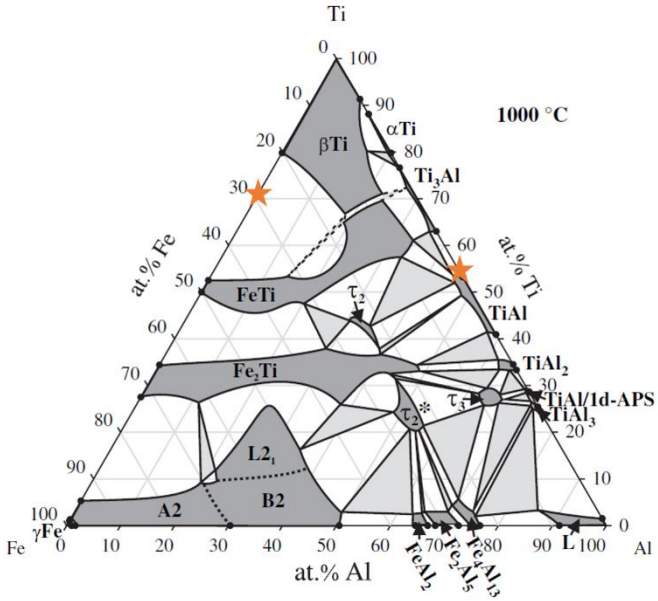

Fig. 6: Phase diagram of Al-Fe-Ti at 1000 °C from [21]. The initial compositions of the brazing solder and the substrate are marked by stars.

The diffraction patterns after 24 h of brazing show superstructure reflections of the β_o phase. Thus, we assume that the composition changes due to further diffusion of the different elements towards the region, where the β_o phase is stable. It is known that the disordered β-Ti structure can become an ordered β_o-Ti(Fe,Al) structure in the right chemical composition range [21]. The fact that the superstructure peaks are weak could on the one hand mean that the ordering is not fully achieved after 24 h. On the other hand, it is reported that Al prefers the same atomic sites as Fe [21]. This results in a similar average electron density of these Fe(Al) sites in comparison to the Ti sites, which leads to weaker β_o superstructure ordering reflections. This will be discussed again in the last passage of this chapter. With extended time at the brazing temperature, the β_o grains have the possibility to grow, which leads to the homogenous big, bright grains in zone I. In addition, zone II, the transition zone, is depleted in Fe in comparison to the middle. Additionally, the Ti content is clearly above the level of the substrate, shown by EDX measurements. Consequently, the chemical composition is placed within the two-phase field $\beta_o+\alpha_2$ after fig. 6 and [21]. After 24 h of brazing the phase analysis in fig. 3b shows β_o and γ phase in the middle. As Schloffer et al. [22] described, γ needles or platelets develop during furnace cooling. Thus, for the composition in the middle a two-phase field $\beta_o+\gamma$ is crossed during cooling after 24 h of brazing, where the precipitation of the γ needles in the microstructure and in the grain boundaries of the β_o grains takes place, fig. 3a. The fact that also reflections of the ω" phase were found will be discussed below.

Only during the additional annealing the chemical composition in zone I changes due to diffusion towards a composition in the two-phase field $\beta_o+\gamma$. This is supported by the fact that the microstructure shows two different morphologies of γ crystallites in fig. 5a. Additional dark globular grains occur (which develop during the annealing process) next to the γ needles already seen in the as-brazed specimen (which arose while cooling). Furthermore, the grain boundaries of the β_o grains are much better visible because additional small globular γ grains are located there. In general, the big β_o grains lead to slow homogenization even after the annealing. The ordered β_o structure slows down the diffusion process in the grains. An additional factor can be that only a small number of

grain boundaries exist which can act as fast diffusion paths. Thus, the homogenization takes place slowly. The amount of α_2 in zone II is higher in the annealed specimen than in the as-brazed one, fig. 5b, which clearly shows the diffusion of Fe from the joint into the substrate. Further homogenization of the joint is visible in the diffusion affected substrate (zone III), as the zone is almost not visible any more after the annealing.

The fact that the HEXRD results show reflections of ω" next to β_o phase (fig. 4) arises from the transformation of β_o into ω_o while cooling [20]. This is not visible in the ternary phase diagram of [21] as the additional Nb is responsible for this transformation. In detail, the transformation process needs an intermediate step from ordered β_o into ω_o via the ω" structure while cooling. The fact that the peaks of the ω" phase occur in the as-brazed specimen with a noticeably width means that very small domains developed. In contrast, the FWHM of the ω" peaks in the annealed specimen is only around half that of the as-brazed condition. The fact that β has to be ordered for transformation into the ω_o structure leads to the assumption that the β_o phase is slightly ordered at the higher brazing temperature of 1110 °C. Consequently, the ordering occurs more distinctly after 168 h at the lower annealing temperature of 1000 °C. The transformation of the slightly ordered β_o phase takes time during furnace cooling of the as-brazed specimen, which leads to small domains of ω" structure. Thus, the transformation into ω" has progressed further in the annealed specimen with stronger ordered β_o crystallites.

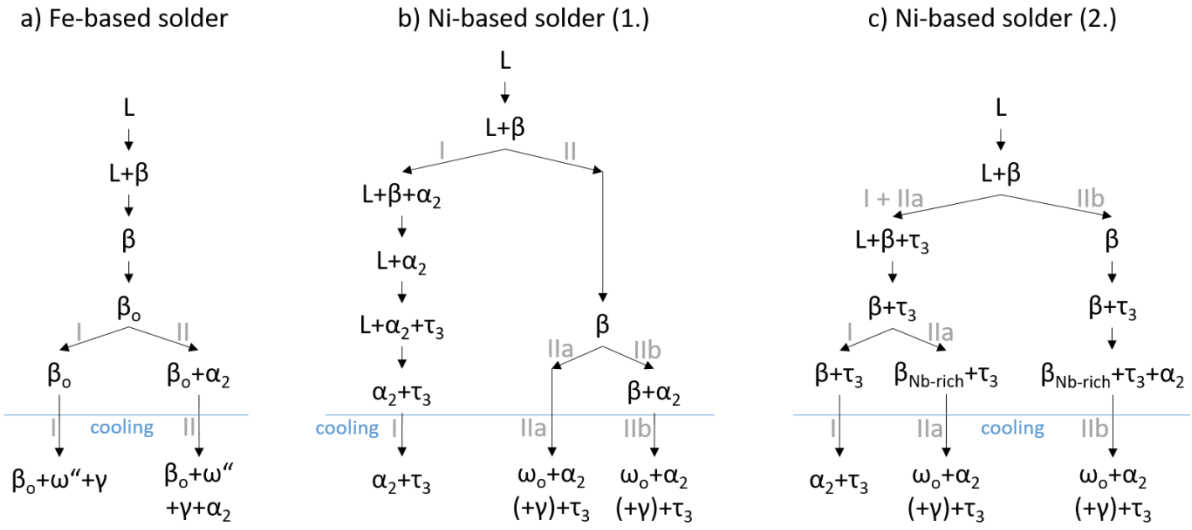

Fig. 7: Flow charts of the different solidification paths with the following solid-state transformations of the two different systems. Two different possibilities are discussed for the Ni-containing system. The different transformation paths are divided into the several zones (I, II(a, b)).

3.5 Results Ni-based solder – as-brazed condition

3.5.1 Microstructure

The microstructure of the joint clearly differs from the substrate material, fig. 8a. The joint region of the as-brazed specimen has a width of 370 µm and no pores or cracks are visible. It appears much brighter in BSE mode than the substrate material due to the higher amount of the heavy elements Ti and Ni compared to the substrate. For further descriptions, the joint is divided into two zones, as marked in fig. 8a. These zones are symmetric on both sides of the joint centre. In the middle of the joint (zone 1) the microstructure shows two rows of large blocky α_2 grains. Additionally, a seam of bright needles appears at the boundaries of these grains, as shown in higher magnification in fig. 9. These needles can be identified as τ_3 phase by HEXRD [23]. The transition zone (zone II) next to the dark seam appears brighter and can be divided into two subzones. In zone IIa bigger areas are visible showing a fine grained, eutectic sub-structure out of α_2 and ω_o [20]. Additionally, small white needles (τ_3 phase) and small, dark precipitates (γ) are noticeable at the grain boundaries. Closer to the substrate in zone IIb, additional light grey globular grains (α_2 phase) are visible. In zone III, the diffusion affected substrate, the grains are larger in comparison to the unaffected substrate. Some additional small white grains (ω_o or τ_3) are also visible.

3.5.2 Phase analysis with HEXRD

The phase composition, fig. 8b, obviously changes with each zone that is present in the microstructure, fig. 8a. The joint consists mainly of α_2 phase, but its fraction differs clearly from zone to zone. The amount increases from the substrate over zone III to zone IIb from 20 vol. % to almost 80 vol. %, decreases slightly in zone IIa and increases again towards the middle which consists almost exclusively of α_2 with about 95 vol. %. In contrast, the amount of γ phase decreases clearly in zone III and is below 5 vol. % in zone IIb. Further, the amount of γ increases slightly in zone IIa and no γ is found in zone I. Furthermore, the ternary ω_o phase is present only in the outer parts of the joint in zone II and III. In parallel, the ternary τ_3 phase is found also mainly in zone II and zone III, but small amounts are as well present in zone I (about 4 vol. %). Both phases increase slightly from the substrate towards zone IIa but decrease again in zone I. The maximum values of ω_o and τ_3 in zone IIa are about 20 vol. % and 8 vol. %, respectively. Unfortunately, it was not possible to resolve the small region between the two α_2 rows in zone I as the synchrotron beam had a size of 50 µm in this direction. Thus, it is not clearly known from the HEXRD measurements whether τ_3 and ω_o are present there, although the appearance of the microstructure leads to this assumption.

3.5.3 Chemical analysis (EDX)

Fig. 8c shows the content of the alloying elements in the different zones of the joint. In general, the amounts of Ti and Ni increase in the joint in comparison to the substrate. In contrast, the contents of Al and Nb decrease in the middle of the joint as those two elements were not part of the composition of the brazing solder. In detail, the content of Ti increases from zone III to zone II, whereas the inner zone IIa contains of a slightly lower amount. The highest content of Ti is found in the blocky α_2 grains in the middle with about 58 at. %. It decreases in the small seam between the α_2 grains in zone I. The amount of Al has increased to about 38 at. % all over the joint. The content of Nb decreases significantly in the blocky α_2 grains, otherwise it stays quite constant over the whole joint and is comparable with that in the substrate. The amount of Ni increases continuously from the substrate to the middle of the joint with the exception of the blocky α_2 grains in zone I, where only 0.6 at. % is measured.

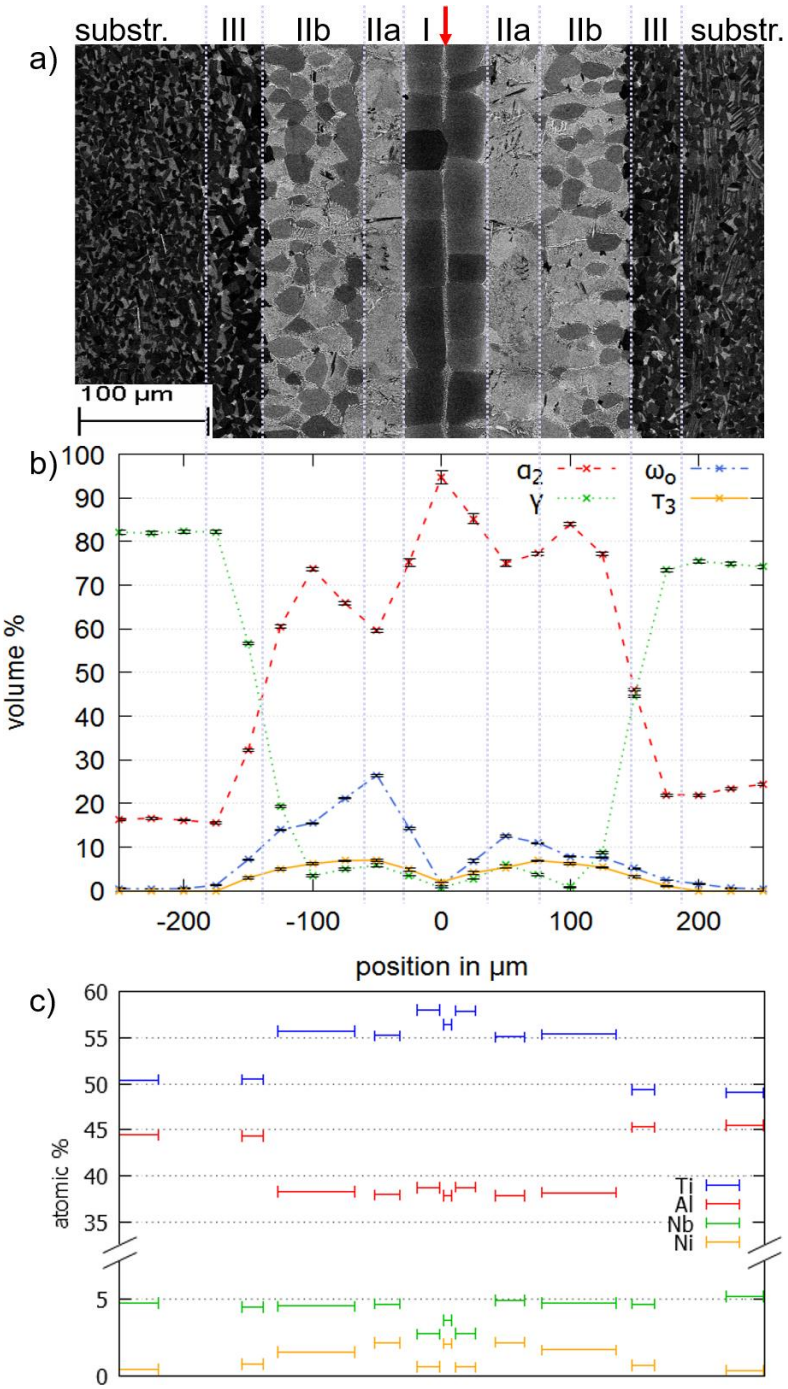

Fig. 8: The results of the Ni-containing as-brazed specimen arranged next to each other a) Microstructure, b) Volume fractions of phases determined by Rietveld analysis of HEXRD measurements, and c) Results of the EDX mappings. The different zones are marked: substr.: substrate, zone I: middle, zone II: transition zone, zone III: diffusion affected substrate. The red arrow marks the middle of the joint.

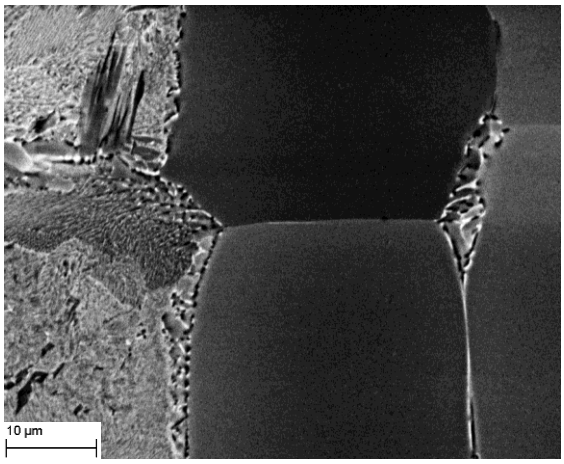

Fig. 9: Microstructure of the middle (zone I and IIa) of the Ni-containing as-brazed joint with higher resolution. The white needles at the grain boundaries are τ_3 phase.

The chemical composition in the small region between the blocky α_2 grains seems to be similar to the one of zone IIa with the exception that the amount of Ti is slightly higher and Nb slightly lower. In detail, the τ_3 needles have a composition of about 45 at. % Ti, 40 at. % Al, 5 at. % Nb, and 10 at. % Ni, which means, that they contain locally the highest amount of Ni found in the whole joint. Furthermore, the composition in the diffusion affected substrate is very similar to the microstructurally unaffected substrate, containing only 0.7 at. % Ni. Remarkably, the concentration of Ni is at least 0.4 at. % in the microstructurally unaffected substrate.

3.6 Results Ni-based solder - annealed condition

3.6.1 Microstructure

After the annealing, the microstructure of the joint region homogenizes significantly and widens from 370 µm to 530 µm, fig. 10a. Additionally, the different zones parallel to the joint are difficult to distinguish, and the diffusion affected substrate (zone III) is not visible anymore. Still, the microstructure shows no pores or cracks in the joint. Mainly, the microstructure in the joint shows globular light grey α_2 grains with smaller dark γ and white τ_3 precipitates in between. Similar to the as-brazed specimen, the dark and white precipitates are located at the grain boundaries of the α_2 grains. In addition, bigger white particles appear in the middle of the joint, which are mostly aligned parallel to the joint. In some cases they are also elongated perpendicular to the joint. It seems, that these white grains are located at the grain boundaries of the former blocky α_2 grains. The particles are not found in the as-brazed specimen. Based on the HEXRD measurements shown below they can be identified as τ_2 phase [24].

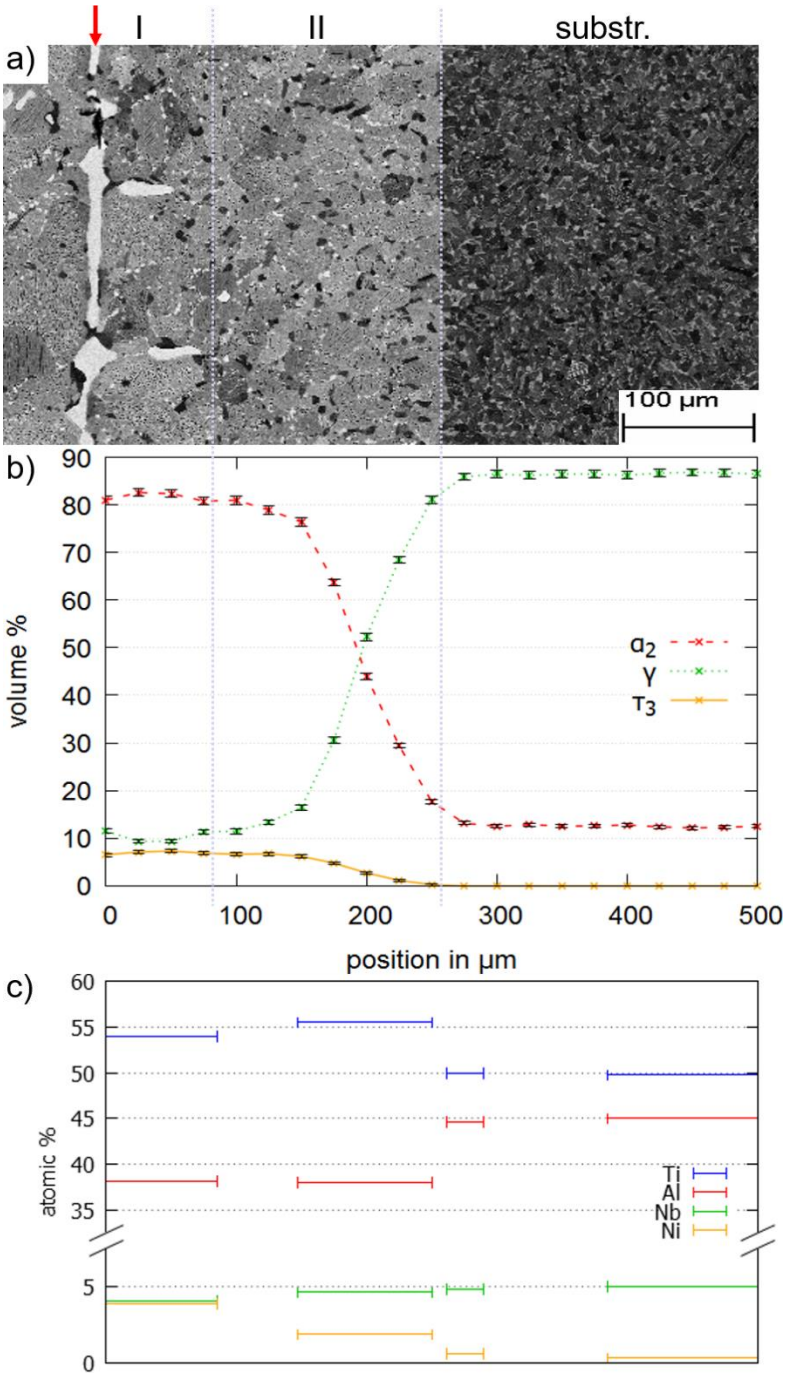

Fig. 10: The results of the Ni-containing annealed specimen arranged next to each other a) Microstructure, b) Volume fractions of phases determined by Rietveld analysis of HEXRD measurements, and c) Results of the EDX mappings. The different zones are marked: substr.: substrate, zone I: middle, zone II: transition zone. Only half of the joint was analysed and is shown here, the red arrow marks the middle of the joint.

3.6.2 Phase analysis with HEXRD

After the annealing process, the ω_o phase is completely dissolved, fig. 10b. The phase composition is nearly constant over zone I and the inner half of zone II, which fits well with the homogeneous appearance of the microstructure. In addition, in the outer part of zone II the phase composition changes slower from the phase composition of the joint to the one of the substrate compared to the as-brazed specimen. Here, the amount of α_2 decreases continuously over 150 µm from more than 80 vol. % to about 15 vol. %. The τ_3 phase still has an amount of about 5 to 10 vol. %, as before the annealing. Additionally, new peaks in comparison to the as-brazed specimen can be related to the τ_2 phase. These are only visible in the middle of the joint, in contrast to the τ_3 phase, which is present over the whole joint region. The diffraction patterns of the τ_2 phase exhibit some single Bragg reflections but no continuous diffraction ring, see fig. 11. Thus, the τ_2 phase can be related to the big, white grains in the middle of the joint, fig. 10a. With this bad grain statistic the Rietveld refinement is not able to determine the fraction of the τ_2 phase, and thus it is not included in fig. 10b. Additionally, the peaks are low in comparison to the ones from the α_2 and even the τ_3 phase.

3.6.3 Chemical analysis (EDX)

As in the as-brazed specimen, the amounts of Ti and Ni are still higher in the joint of the annealed specimen, fig. 10c, in comparison to the substrate. In parallel, the contents of Al and Nb still decrease towards the centre of the joint. In zone II almost the same chemical composition is found as in the as-brazed specimen in zone IIa next to the blocky α_2 grains. Furthermore, the composition of the τ_2 grains is determined to be 33.1 at. % Ti, 43.2 at. % Al, 3.2 at. % Nb, and 20.5 at. % Ni, which is chemically closer to the composition of τ_3 in comparison to the composition of τ_2 with the high content of Ti. This is also remarkable as it is almost the amount of Ni of the initial brazing solder. The content of Ni increases in zone I compared to the as-brazed specimen (fig. 8c), but this effect is more due to different selection of the measured regions by EDX. In the as-brazed specimen the grain boundaries with a high amount of white Ni-rich τ_3 needles were not analysed as the composition of the single zones should be determined by the measurement. The amount of Ni decreases to 0.6 at. % in the region, which corresponds to the diffusion affected substrate in the as-brazed specimen. Additionally, an amount of 0.3 at. % Ni is measured in the microstructurally unaffected substrate, which is comparable to the as-brazed specimen.

3.7 Discussion Ni-based solder

Obviously, the elements Al and Nb stem from the substrate and enter the joint by dissolution of substrate in the beginning of the brazing process and by diffusion. They reach a nearly constant level over the whole joint with the exception of the blocky α_2 grains (zone I) in the as-brazed specimen. Furthermore, the amounts of Ti and Ni decrease in comparison to the initial composition of the brazing solder in the joint also due to dissolution of the substrate and diffusion.

Unfortunately, no reliable Al-Ni-Ti phase diagram at 1100 °C is available and in the phase diagram at 1000 °C, published by Schuster et al. [25], the Ti-rich edge is missing. Thus, an assumption about the ternary phase diagram Al-Ni-Ti at 1100 °C has to be made for an explanation of the microstructure development of the as-brazed joint, fig. 8a. We found two different possible explanations for the microstructure after the brazing with different phase transformation paths during the brazing process. They will be discussed in the following and are additionally shown as flow charts in fig. 7b and 7c.

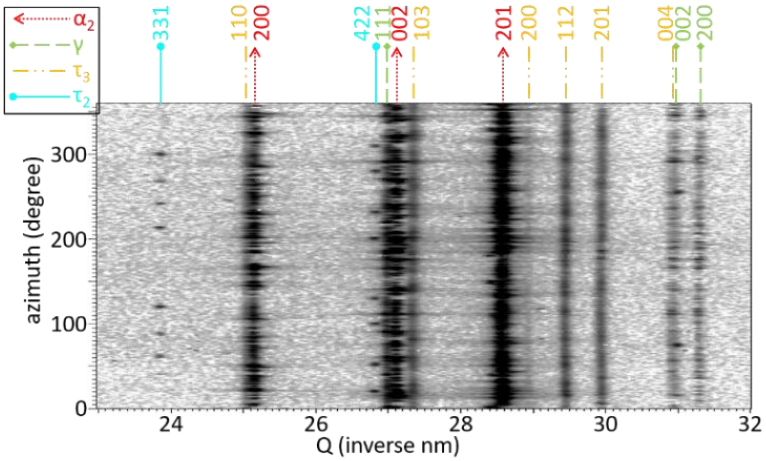

Fig. 11: The unrolled Debye-Scherrer diffraction rings from one measurement out of the middle (zone I) of the Ni-containing annealed joint with the marked phases α_2, γ, τ_3, and τ_2.

3.7.1 Solidification via two steps - β and α_2

According to [26] the single β phase field in the Ti-rich corner is assumed to be rather big as visible in the sketch in fig. 12a. Consequently, the three-phase field L+β+α_2 is assumed to be rather small compared to the surrounding phase fields. The transformation path is shown in fig. 7b.

After the brazing temperature is reached, the brazing solder melts and dissolves the adjacent substrate. Then, the concentration of the melt moves toward increasing Al and Nb contents and decreasing Ti and Ni contents. The composition of the melt changes until it reaches the liquidus surface to the two-phase field L+β. This leads to dendrites of β phase growing perpendicular to the substrate in zone II (light grey grains). Subsequently, the composition of the liquid moves along the liquidus surface with increasing Al and decreasing Ti and Ni contents and hits the edge of the three-phase field L+β+α_2. As shown in fig. 12a, this field is assumed to be rather small. Thus, the composition changes nearly directly into the two-phase field L+α_2. This leads to an abrupt change of the type of precipitation out of the liquid from β to α_2 crystallites and to the division into the two zones. In zone I the composition changes from L+α_2 towards the three-phase field L+α_2+τ_3 due to further increasing Al and decreasing Ti contents. Finally, the remaining liquid crystallizes as fine grained α_2+τ_3 at the grain boundaries of the big α_2 grains. In zone II the composition changes from L+β to the single β phase field due to further diffusion. Furthermore, in the outer part of this zone (zone IIb) the composition changes towards the two-phase field β+α_2 as the substrate, which provides Al and consumes Ti and Ni, is nearby. This results in the globular dark grey α_2 grains in zone IIb and leads to the division of zone II into the two subzones. In the inner zone (zone IIa) the composition stays in the single phase field of β, which results in the light grey grains in the microstructure without any α_2 phase. Thus, the whole joint fully solidifies over time in zone I with α_2 and τ_3 phase and in zone II with β (and in zone IIb additionally α_2 phase). This means, the solidification path leads to a two-stage precipitation and resulting different solid-state transformations in the joint. Afterwards, the grains of β and α_2 grow in both zones during the remaining time of the brazing process. As the concentration of Ni is still high in the centre of the joint it further diffuses towards the substrate. This diffusion probably takes place along the grain boundaries, which explains the existence of Ni-rich τ_3 phase at the grain boundaries over the whole joint. During cooling at the end of the brazing process, the β phase in zone II completely decomposes

into α_2, ω_o, and a small amount of γ. These phases were measured with HEXRD at room temperature after 24 h of brazing, fig. 8b.

3.7.2 Solidification via one step - β

In contrast to the first explanation, no binary phase field L+α_2 is visible in the calculated phase diagram of [27] at 1200 °C and in one calculated with Thermocalc using the TCNI8 Ni-database, fig. 12b. What is found instead is the binary phase field β+τ_3. According to such phase diagrams the composition, after the brazing solder completely liquefies, is assumed to stay in the two-phase field L+β, fig. 7c. Subsequently, in the main joint region (zone I and zone IIa) the composition changes into the three-phase field L+β+τ_3 and further in the two-phase field β+τ_3. The Ni enriches at the grain boundaries of β, which leads to τ_3 phase precipitation there. The phase composition in zone IIb next to the substrate changes due to easier diffusion of Ni towards the substrate into the single β phase field and due to further diffusion into the phase fields β+τ_3 and β+τ_3+α_2. Nb has to diffuse in from the substrate over the whole brazing process (with the exception of the first step of dissolution of the substrate). It seems that the transition from zone I to zone II marks the diffusion front of Nb from the substrate to the middle of the joint after 24 h of brazing, which is revealed by the EDX measurements, fig. 8c. Thus, while cooling the Nb-lean β grains in zone I transform to α_2 grains and the Nb-rich β grains in zone II decompose into α_2, a small amount of γ, and ω_o, as Nb is known to be an ω_o stabilizer [20].

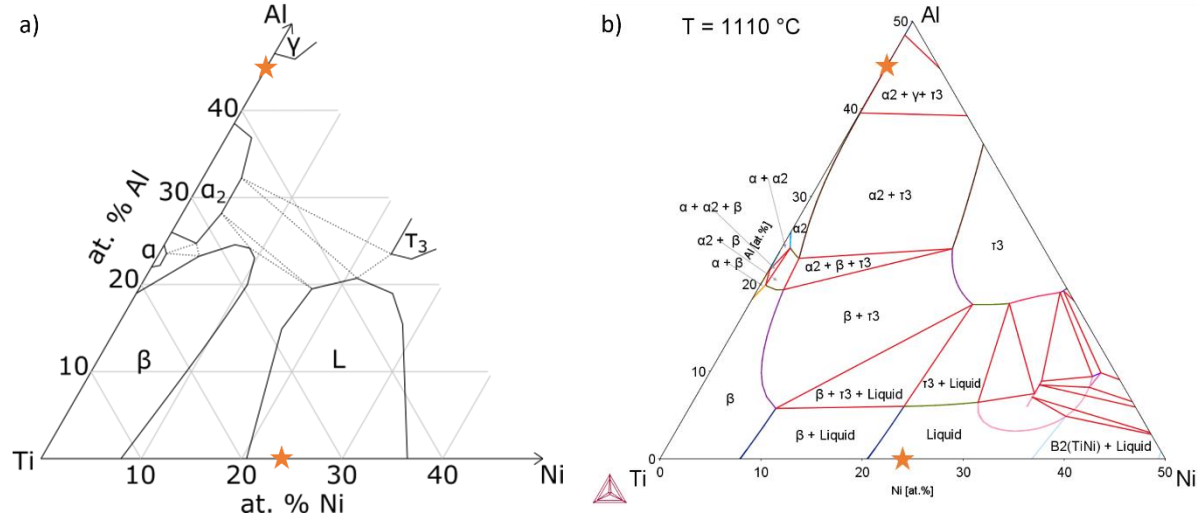

Fig. 12: Phase diagram of Al-Ni-Ti, a) hypothetical phase diagram at 1110 °C, b) Calculated phase diagram using the thermodynamic Ni-database TCNI8 with Thermocalc. The initial compositions of the brazing solder and the substrate are marked.

3.7.3 Additional annealing

After the annealing α_2, τ_3, and some amount of γ phase were detected in zone II. Due to further diffusion during the additional annealing (decreasing Ti and increasing Al) the joint homogenizes and thus the ω_o phase in zone II dissolves. This leads to α_2+τ_3+γ being present in zone II after annealing at 1000 °C, which is in agreement with the chemical composition determined by EDX and the phase constitution predicted by the corresponding ternary phase diagram of Al-Ni-Ti [25]. The τ_2 phase in the middle of the joint after the annealing exhibits a chemical composition related to the τ_3 phase, but the crystallography is clearly identified as τ_2. In detail, the measured chemical composition of the τ_2 phase is determined to be near the phase boundary between the single τ_3 phase field and the two-phase field of τ_3+τ_2 in the ternary Al-Ni-Ti phase diagram at 1000 °C [25]. This disregards any possible

effects of Nb. The amount of about 5 at. % Nb might lead to a shift of the phase boundaries and thus justifies the high amount of τ_2 phase which is visible in the microstructure in the middle of the annealed joint. In general, compounds of γ and α_2 exhibit a low solubility for Ni (α_2 in equilibrium with γ dissolves only 0.9 at. % Ni at 900 °C and γ dissolves only 0.8 at. % Ni at 1000 °C) [25, 28]. Consequently, Ni seems to enrich in the ternary τ_3 phase or after the annealing in both ternary τ_2 und τ_3 phases in the grain boundaries.

3.8 Comparison of Fe-based and Ni-based solder

The two different MPDs (Fe and Ni) lead to clearly different microstructures. The joint region of the Ni-containing joint is wider than the Fe-containing one, especially after the annealing process. This might be due to the fact, that the diffusion coefficient of Ni in γ-TiAl at 1000 °C is more than 1.5 times higher than the one of Fe. In detail, they amount to 2.02 * 10^{-16} m^2/s and 1.29 * 10^{-16} m^2/s for Ni and Fe, respectively [29]. In general, the Fe-containing joint exhibits big β_o grains, which are still visible with approximately the same size after the annealing. In contrast, the Ni-containing joint has a finer grained microstructure especially after the annealing. After annealing, even the sub-division of the transition zone II and the blocky α_2 grains are not visible anymore. This indicates a better homogenization of the microstructure after the annealing. Furthermore, only phases that are found in the TiAl system were observed in the Fe-containing joint. All of them are still present after the annealing with their amounts being closer to the phase composition of the substrate. In contrast, additional ternary phases (τ_3 and τ_2) are present in the Ni-containing joint. Furthermore, the ω_o phase has disappeared in the Ni-containing joint after the annealing, which indicates homogenization. We discussed, that the Fe-containing joint solidifies via the single β_o phase field, which leads to the big β_o grains. In contrast, the Ni-containing joint solidifies at least in a two-phase field ($\beta+\tau_3$ or $\alpha_2+\tau_3$), which might lead to the finer grained microstructure. The phase composition of the Ni-containing joint seems to be influenced more by the chemical gradient compared to the Fe-containing system. This fits well with the different phase diagrams available in literature or predicted by thermodynamic calculation. Remarkably, the averaged amounts of the single elements show the same behaviour over the joint in both systems. In the joints more Ti and MPD is found, but already an amount of 35 to 40 at. % Al is measured, which stems from diffusion out of and dissolution of the substrate. Additionally, on average only about 5 at. % of the particular MPD remains in the middle of the joints. Furthermore, Fe seems to be located in the main crystallites of β phase, whereas, Ni seems to enrich in the remaining liquid, which leads to the Ni-rich τ phases at the grain boundaries. In general, the Ni-containing joint seems to be better homogenized and should be preferred especially due to the finer grained microstructure. Nevertheless, the influence of the small amounts of ternary τ phases needs further investigations.

4. Conclusion

A third generation γ-TiAl alloy was successfully brazed by transient liquid phase bonding with two different brazing solders. Ni and Fe were chosen as the two different MPDs, which led to quite different results. One set of specimens was brazed for 24 h at 1110 °C, another set was additionally annealed for 168 h at 1000 °C after the brazing process. The joints were investigated with HEXRD and additionally with scanning electron microscopy with EDX. The HEXRD data was analyzed by Rietveld refinement. Conclusions are summarized as follows:

a) The microstructures of the joints show two different zones with different phase compositions. Additionally, a zone of diffusion affected substrate is visible next to the joint. The different zones are arranged symmetrical on both sides of the joint. After annealing, the microstructure only changes significantly in the Ni-containing system, but both joint regions grow wider. Generally, the amount of γ phase decreases from the substrate to the joint in both systems, and additional phases not present in the substrate can be found in the joints.

b) The joint of the Fe-containing joint solidifies in the single β_o phase field, which leads to large, blocky β_o grains in the joint. After annealing the amounts of α_2 and γ increase, but the whole joint is slightly better homogenized. In both cases, the Fe is distributed homogeneously over the whole joint in the β_o grains. Needles of γ phase form while cooling. Additionally, reflections of small ω" domains are also identified after cooling. Only phases known from γ-TiAl alloys are observed.

c) The finer grained Ni-containing joint solidifies at least in a two-phase field of $\beta+\tau_3$ or $\alpha_2+\tau_3$. After cooling, the joint mainly consists of α_2 phase with τ_3 at the grain boundaries. Additional ω_o phase is only present in the as-brazed specimen. We discussed two different possibilities for the development of the microstructure after the brazing. The microstructure clearly homogenizes after annealing. The MPD Ni enriches in the ternary phase τ_3 and after the annealing also in the τ_2 phase. The Ni-containing system seems to be more sensitive to chemical gradients.

Appendix: Crystallographic data of all phases measured in the specimens.

Phase	Pearson symbol	Space group	Struktur-bericht	Wyckoff positions	lattice parameter in angstrom	reference
α_2-Ti_3Al	hP8	$P6_3/mmc$, #194	DO_{19}	2d:Al 6h:Ti	a = 5.765 c = 4.625	[1]
γ-TiAl	tP4	P4/mmm, #123	$L1_0$	1a: Al 1c: Al 2e: Ti	a = 4.016 c = 4.068	[1]
β-Ti(Al,Nb)	cI2	Im-3m, #229	A2	1a: Ti, Al, Nb	a = 3.307	[1]
β_o-TiAl(Nb)	cP2	Pm-3m, #221	B2	1a: Ti 1b: Al, Nb	a = 3.216	[1]
ω”-Ti_4Al_3Nb	hP6	P-3m1, #164		1a: Ti 1b: Nb, Al $2d_1$: Al $2d_2$: Ti	a = 4.58 c = 5.52	[20]
ω_o-Ti_4Al_3Nb	hP6	$P6_3/mmc$, #194	$B8_2$	2a: Ti, Al, Nb 2c: Al 2d: Ti	a = 4.580 c = 5.520	[20]
τ_3-Al_3NiTi_2	hP12	$P6_3/mmc$, #194	C14	2a: Ni 4f: Ti 6h: Al	a = 4.990 c = 8.040	[23]
τ_2-Al_2NiTi	cF116	Fm-3m, #225	$D8_4$	4a: Ni 4b: Al 24d: Ni 24e: Ti $32f_1$: Al $32f_2$: Al	a = 11.5	[24]
TiB	oP8	Pnma, #62	B27	4c: B 4c: Ti	a = 6.110 b = 3.050 c = 4.560	[1]
FeTi	cP2	Pm-3m, #221	B2	1a: Cs 1b: Cl	a = 2.988	[15, 16]
α-Ti	hP2	$P6_3/mmc$, #194	A3	2c: Ti	a = 2.952 c = 4.683	[15]
Ti_2Ni	cF96	Fd-3m, #227	---	16d: Ti 32e: Ni 48f: Ti	a = 11.338	[15]

References:

[1] F. Appel, J.D.H. Paul, M. Oehring, Gamma Titanium Aluminide Alloys, Wiley-VCH, Weinheim, 2011.
[2] H. Clemens, S. Mayer, Design, Processing, Microstructure, Properties, and Applications of Advanced Intermetallic TiAl Alloys, Adv. Eng. Mater. 15(4) (2013) 191-215.
[3] P. Heinz, A. Volek, R.F. Singer, M. Dinkel, F. Pyczak, M. Goken, M. Ott, E. Affeldt, A. Vossberg, Diffusion brazing of single crystalline nickel base superalloys using boron free nickel base braze alloys, Defect. Diffus. Forum 273-276 (2008) 294-299.
[4] K. Nishimoto, K. Saida, D. Kim, S. Asai, Y. Furukawa, Y. Nakao, Bonding phenomena and joint properties of transient liquid phase bonding of Ni-base single crystal superalloys, Weld. World 41 (1998) 121-131.
[5] D.U. Kim, K. Nishimoto, Bonding phenomena of transient liquid phase bonded joints of a Ni base single crystal superalloy, Met. Mater.-Int. 8(4) (2002) 403-410.
[6] D.S. Duvall, W.A. Owczarski, D.F. Paulonis, TLP Bonding - a New Method for Joining Heat-Resistant Alloys, Weld. J. 53(4) (1974) 203-214.
[7] S. Neumeier, M. Dinkel, F. Pyczak, M. Goken, Nanoindentation and XRD investigations of single crystalline Ni-Ge brazed nickel-base superalloys PWA 1483 and Rene N5, Mater. Sci. Eng. A-Struct. 528(3) (2011) 815-822.
[8] M.K. Dinkel, P. Heinz, F. Pyczak, A. Volek, M. Ott, E. Affeldt, A. Vossberg, M. Goken, R.F. Singer, New boron and silicon free single crystal-diffusion brazing alloys, in: R.C. Reed, K.A. Green, P. Caron, T.P. Gabb, M.G. Fahrmann, E.S. Huron, S.A. Woodard (Eds.), Superalloys 2008, Minerals, Metals & Materials Soc, Warrendale, 2008, pp. 211-220.
[9] K. Hauschildt, A. Stark, U. Lorenz, N. Schell, T. Fischer, M. Blankenburg, M. Müller, F. Pyczak, Diffusion brazing of γ-TiAl-alloys: Investigations of the joint by electron microscopy and high-energy X-ray diffraction, Mater. Res. Soc. Symp. P. 1516 (2013) 215-220.
[10] H. Duan, M. Kocak, K.H. Bohm, V. Ventzke, Transient liquid phase (TLP) bonding of TiAl using various insert foils, Sci. Technol. Weld. Join. 9(6) (2004) 513-518.
[11] X.G. Song, J. Cao, H.Y. Chen, Y.F. Wang, J.C. Feng, Brazing TiAl intermetallics using TiNi-V eutectic brazing alloy, Mater. Sci. Eng. A-Struct. 551 (2012) 133-139.
[12] T.S. Lin, H.X. Li, P. He, H.M. Wei, L. Li, J.C. Feng, Microstructure evolution and mechanical properties of transient liquid phase (TLP) bonded joints of TiAl intermetallics, Intermetallics 37 (2013) 59-64.
[13] A. Guedes, F. Viana, A.M.P. Pinto, M.F. Vieira, Diffusion Brazing of a gamma-TiAl Alloy Using Tini 67: Microstructural Evolution of the Interface, Mater. Sci. Forum 587-588 (2008) 425-429.
[14] W.F. Gale, D.A. Butts, Transient liquid phase bonding, Sci. Technol. Weld. Join. 9(4) (2004) 283-300.
[15] J.L. Murray (Ed.), Phase diagrams of binary titanium alloys, ASM International, Metals Park, 1987.
[16] H. Okamoto, Fe-Ti (iron-titanium), J. Phase Equilib. 17(4) (1996) 369-369.
[17] N. Schell, A. King, F. Beckmann, T. Fischer, M. Müller, A. Schreyer, The High Energy Materials Science Beamline (HEMS) at PETRA III, Mater. Sci. Forum 772 (2014) 57-61.
[18] A.P. Hammersley, FIT2D: a multi-purpose data reduction, analysis and visualization program, J. Appl. Crystallogr. 49 (2016) 646-652.
[19] L. Lutterotti, Total pattern fitting for the combined size-strain-stress-texture determination in thin film diffraction, Nucl. Instrum. Meth. B 268(3-4) (2010) 334-340.
[20] A. Stark, M. Oehring, F. Pyczak, A. Schreyer, In Situ Observation of Various Phase Transformation Paths in Nb-Rich TiAl Alloys during Quenching with Different Rates, Adv. Eng. Mater. 13(8) (2011) 700-704.
[21] M. Palm, J. Lacaze, Assessment of the Al-Fe-Ti system, Intermetallics 14(10-11) (2006) 1291-1303.
[22] M. Schloffer, B. Rashkova, T. Schoberl, E. Schwaighofer, Z.L. Zhang, H. Clemens, S. Mayer, Evolution of the omega(o) phase in a beta-stabilized multi-phase TiAl alloy and its effect on hardness, Acta Mater. 64 (2014) 241-252.

[23] B. Huneau, P. Rogl, K. Zeng, R. Schmid-Fetzer, M. Bohn, J. Bauer, The ternary system Al-Ni-Ti Part I: Isothermal section at 900 degrees C; Experimental investigation and thermodynamic calculation, Intermetallics 7(12) (1999) 1337-1345.
[24] A. Grytsiv, J.J. Ding, P. Rogl, F. Weill, B. Chevalier, J. Etourneau, G. Andre, F. Bouree, H. Noel, P. Hundegger, G. Wiesinger, Crystal chemistry of the G-phases in the systems Ti-{Fe, Co, Ni}-Al with a novel filled variant of the Th6Mn23-type, Intermetallics 11(4) (2003) 351-359.
[25] J.C. Schuster, Z. Pan, S.H. Liu, F. Weitzer, Y. Du, On the constitution of the ternary system Al-Ni-Ti, Intermetallics 15(9) (2007) 1257-1267.
[26] J. Bursik, P. Broz, Constitution of Ni-Al-Ti system studied by scanning electron microscopy, Intermetallics 17(8) (2009) 591-595.
[27] K. Zeng, R. Schmid-Fetzer, B. Huneau, P. Rogl, J. Bauer, The ternary system Al-Ni-Ti Part II: Thermodynamic assessment and experimental investigation of polythermal phase equilibria, Intermetallics 7(12) (1999) 1347-1359.
[28] L.I. Duarte, C. Leinenbach, U.E. Klotz, M.C.J. Marker, K.W. Richter, J.F. Loffler, Experimental study of the FeAl-NiAl-TiAl section, Intermetallics 23 (2012) 80-90.
[29] C. Herzig, T. Przeorski, M. Friesel, F. Hisker, S. Divinski, Tracer solute diffusion of Nb, Zr, Cr, Fe, and Ni in gamma-TiAl: effect of preferential site occupation, Intermetallics 9(6) (2001) 461-472.